*Article*

# Design of High-Dynamic PMSM Servo Drive Using Nonlinear Predictive Controller with Harmonic Disturbance Observer

Zhanqing Zhou [1], Shuaijiang Yao [1], Chaolei Ma [2], Guozheng Zhang [1,*] and Qiang Geng [1,*]

[1] School of Electrical Engineering, Tiangong University, Tianjin 300387, China; zhzhq@tju.edu.cn (Z.Z.); 20170021@tiangong.edu.cn (S.Y.)
[2] School of Electrical and Information Engineering, Tianjin University, Tianjin 300387, China; machaolei@tju.edu.cn
* Correspondence: zhanggz@tju.edu.cn (G.Z.); gengqiang@tju.edu.cn (Q.G.)

**Abstract:** The high-dynamic permanent magnet (PM) motor servo system with high-bandwidth is the core equipment for industrial production, and the control bandwidth is also an important indexes to evaluate the performance of the servo system. The non-cascaded direct predictive speed control is an appropriate scheme to optimize the dynamic performance of the PM motor servo system. However, the high bandwidth of the non-cascaded control structure results in poor anti-interference ability, and it cannot effectively deal with the coupling relationship between current and speed, leading to poor control performance in the current limit region. Regarding the above problems, a nonlinear predictive speed control strategy combined with harmonic disturbance observer is proposed. In the proposed strategy, the disturbances of the servo system are separated from the mathematical model according to the nonlinear modeling theory, and the traditional disturbance observer is modified to estimate the harmonics. A nonlinear control law with strong disturbance suppression ability was designed. Furthermore, a complete current and speed prediction mechanism was introduced into the algorithm, in which the proportional differential (PD) controller is employed as the connection medium between the reference current and speed to solve the coupling problem of the non-cascaded control structure.

**Keywords:** model predictive control; nonlinear observer; disturbances attenuation; permanent magnet synchronous motor (PMSM); observer-based control

## 1. Introduction

High precision servo control has been widely used in computer numerical control (CNC) machines, artificial intelligence, etc. Because permanent magnet (PM) motors have the advantages of simple structure, high specific power, and wide speed range [1,2], they are usually employed as the main motor system of servo control. The speed control algorithm of the PM servo system usually adopts the cascade control structure with the current inner loop and the speed outer loop. This control structure requires that the control bandwidth of the current loop is much larger than that of the speed loop, to meet the stability condition of system, resulting in the limitation of the dynamic response speed of the motor [3–5]. To match the growing demand for highly dynamic and high-precision modern servo systems, the non-cascaded direct predictive speed control (DPSC) has become an important research direction in servo system control strategy [6,7]. Because of its excellent dynamic performance and multivariable online optimization abilities, DSPC is an appropriate scheme to construct the direct speed control structure of a PM servo motor [8,9].

In recent years, the model predictive control algorithm has achieved great success in the permanent magnet synchronous motor (PMSM) drive, which improves the dynamic performance of the motor drive system [10,11]. DPSC is a feasible means of further optimizing the dynamic performance of the PM servo system. Currently, scholars are trying

to improve DPSC in terms of the two aspects of disturbance suppression and efficient operation, so as to make it possible for industrial application.

The excellent dynamic performance of DPSC is due to its high-bandwidth characteristics; however, the anti-interference capability of this high-bandwidth control structure is relatively weak. There are a large number of harmonics in the servo system, causing the problems of parameter mismatch, machining error, and control misalignment. A high-bandwidth structure cannot effectively suppress these medium- and high-frequency harmonics, resulting in the deterioration of the steady-state performance [12,13]. To solve this problem, a repetitive controller is embedded into the model predictive control (MPC) algorithm according to the Fourier series, which is equivalent to adding periodic motion modes to the controller. This improves the suppression ability of the MPC to the corresponding periodic disturbance [14]. Similarly, an iterative learning MPC controller was proposed in [15]. Compared with the repetitive MPC or iterative learning MPC, the frequency characteristic of the resonant controller is more stable and has less impact on the stability of the control system. On this basis, the predictive-resonant controller is formed by integrating multiple resonant units into the MPC, which enhances the control ability of the controller to the signal at a specific frequency [16,17]. However, DPSC is a typical multiple input and multiple output (MIMO) controller. Both repetitive MPC and resonant MPC algorithms adopt the design idea of a single input and single output (SISO) controller, which is not suitable for the design of DPSC. The robust MPC controller is a kind of MIMO MPC strategy, and is suitable for the transformation to DPSC [18–20]. Instead of the accurate frequency information of disturbances, the key control information of the robust MPC is only the extreme range of disturbances. For this reason, the robust MPC can only satisfy the minimum control objectives (such as tracking and stability) in the presence of disturbances. Due to its simple structure, intuitive principle, and suitability for MIMO design, the observer-based MPC (OB-MPC) is a sophisticated methods to suppress disturbances in a control system that adopts a predictive algorithm [21–23]. According to the estimated value of the observer, this kind of algorithm will generate supplementary values that can be directly superimposed in the control quantity, so as to improve the control performance. However, these algorithms pay more attention to the estimation and suppression of constant disturbances [24], and fewer reports have been made about the application of the algorithms to harmonic disturbances.

The cascade control structure is abandoned in DPSC, resulting in the disappearance of the direct relationship between speed and current. Thus, it is difficult to utilize the maximum operation current of the motor for DPSC, due to considerations of safe operation and stability. Specifically, assuming that the motor boundary constraint is too strict, the motor cannot reach its maximum efficiency; otherwise, the transient current of the motor will be large, which means that it is easy to trigger an overcurrent fault. To solve the above problem, an additional current limiting loop is introduced into the output [25–28]. However, this method is equivalent to re-imposing a constraint boundary on the solution of an unconstrained optimization problem, which deviates from the actual optimal solution. Hence, the dynamic performance of the servo system will be degraded when tracing the reference, such as a slope signal or acceleration signal. Thus, the current limiting loop is rejected in favor of a PI compensation link, which provides a new idea to deal with the operation problem of DPSC on the current boundary [29]. Due to the integral saturation phenomenon of PI controller, this algorithm needs to be improved further. The explicit model predictive algorithm can suitably deal with the above problems, using different control laws under different control partitions [30,31]. However, the huge number of control partitions increases the difficulty of the algorithm implementation. Therefore, alternative direct speed optimization algorithms without a current limiting link should be researched, under the condition of meeting the computing power of existing microprocessors [32,33]. This would be of great value to the promotion of DPSC.

Aiming at addressing the problems of DPSC in terms of disturbance suppression and efficient operation, a nonlinear predictive speed control strategy combined with harmonic

disturbance observer (HDO-NPSC) is proposed for the design of a PM servo system with high dynamic response and high operation accuracy. In the proposed strategy, the disturbances in the servo system are separated from its classical model according to the nonlinear modeling theory, and the corresponding predictive model including harmonic and constant disturbances is constructed. Then, the nonlinear predictive control law suitable for PM servo system is established by solving the given cost function. In addition, the observer, which can effectively observe the harmonic disturbances of the system, was designed, and the observation values were introduced into the control law to improve the suppression ability of the proposed algorithm, so as to eliminate the control problems caused by non-ideal modeling factors, such as parameter mismatch and control inaccuracy. In contrast to the existing DPSC strategies, the output variables of HDO-NPSC completely include the motor current and speed variables, and a PD controller is used to connect the speed errors and current reference. Hence, HDO-NPSC can employ the maximum working current of the motor without the help of a current limiting link, by appropriately distributing the weight coefficient.

## 2. Harmonics Problem of PMSM Servo Drive

The speed fluctuations of a PM servo motor mainly come from the non-ideal modeling factors in the system, including the parameter mismatch of the motor, the dead-time effect of the converter, and the current sampling errors of the controller.

### 2.1. Parameter Mismatch

The value of the stator resistance is affected by the external environment temperature, and the actual resistance of motor at a given temperature can be expressed with the resistance coefficient $\alpha$, as [34,35]:

$$R_{\text{s}} = R_{\text{s}0}[1 + \alpha(Temp. - 20)], \tag{1}$$

Considering that the value of $\alpha$ is small, and usually selected as 0.00393 ppm/°C, it can be approximately supposed that there is only a constant disturbance in $R_{\text{s}}$, that is:

$$R_{\text{s}} = R_{\text{s}0} + \Delta R, \tag{2}$$

The stator inductance of the motor can be calculated by the finite element method, and its calculation expression is [36]:

$$L_{\text{s}} = \frac{2L_{\text{ef}}\sum_{l=1}^{\infty} H_l B_l \Delta S_l}{3i_{\text{s}}^2}, \tag{3}$$

When the magnetic circuit of the motor is unsaturated, the energy in the magnetic field is stable, and the inductance value will not change greatly. In other words, the nominal value of inductance will only change significantly after the saturation of the magnetic circuit. Therefore, it can still be considered that there are only constant disturbances for the inductance parameter, i.e.,

$$\begin{cases} L_{\text{d}} = L_{\text{d}0} + \Delta L_{\text{d}} \\ L_{\text{q}} = L_{\text{q}0} + \Delta L_{\text{q}} \end{cases}, \tag{4}$$

The moment of inertia of the PM servo system is composed of the motor and the load; its calculation expression is [37]:

$$J_{\text{m}} = \underbrace{\frac{1}{2}\left[M_{\text{iron}}c\left(R_{\text{iron}}^2 + r_{\text{iron}}^2\right) + M_{\text{shaft}}R_{\text{shaft}}^2\right]}_{Motor} + J_{\text{Load}}, \tag{5}$$

From (5), the moment of inertia of the motor can be calculated according to the design parameters. However, it is usually difficult to obtain the load inertia; as a result, the

estimated value of the servo system deviates from its actual value. However, the moment of inertia only depends on the shape of the object, the mass distribution, and the position of the rotation axis, so it can be considered that there is only a constant estimation deviation for $J_m$, that is:

$$J_m = J_{m0} + \Delta J, \tag{6}$$

In the process of system modeling, the permanent flux $\psi_f$ is usually considered to be a constant value, that is, the rotor flux is assumed to be an ideal sinusoidal distribution in space. However, due to the influence of stator slotting, core material saturation, manufacturing process constraints, etc., it is difficult to achieve an ideal sinusoidal distribution in the permanent flux, which leads to the existence of harmonics in the stator winding. The harmonics of the permanent magnet flux linkage in the d-q synchronous coordinates can be expressed as [12]:

$$\begin{cases} \psi_{fd} = \psi_{d0} + \sum_{l=1}^{\infty} \psi_{d6,l} \cos(6l\omega_e t) \\ \psi_{fq} = \sum_{l=1}^{\infty} \psi_{q6,l} \cos(6l\omega_e t) \end{cases}, \tag{7}$$

It can be seen from (7) that subharmonics with $6l\omega_e$ can be found in the permanent magnet, which are represented as $\psi_{d6,l}$ and $\psi_{q6,l}$.

### 2.2. Dead-Time Effects and Current Sampling Errors

Avoiding the operation faults of a voltage sourced inverter, a dead time is usually added to the IGBT control signal, which leads to the deviation in the output voltage. This deviation voltage can be expressed as [38]:

$$\Delta u_x = -\text{sign}(i_x) \frac{T_{dead}}{T_s} u_{dc}, \tag{8}$$

According to the Park transformation, the deviation voltages of A, B, and C phases can be transformed into the d-q frame, which can be expressed as:

$$\begin{cases} \Delta u_{d,dead} = \frac{4T_d u_{dc}}{\pi T_s} \sum_{l=1}^{\infty} \frac{12l \sin(6l\omega_e t)}{36l^2 - 1} \\ \Delta u_{q,dead} = \frac{4T_d u_{dc}}{\pi T_s} \left\{ -1 + \sum_{l=1}^{\infty} \frac{2 \cos(6l\omega_e t)}{36l^2 - 1} \right\} \end{cases}, \tag{9}$$

From (9), when the motor operates stably with the frequency of $\omega_e$, the deviation voltage contains the harmonic disturbances with the frequency of $6l\omega_e$ ($l = 1, 2, 3, \ldots$).

The stator current is the necessary information for the feedback control, and its measurement process includes sensor detection, low-pass filtering, polarity conversion, and analog-to-digital conversion. However, offset errors exist in this measurement because of the imbalanced power supply of the current sensors. In addition, proportional errors will also be detected, as the value of the sampling resistance changes with temperature. To summarize, the current measurement results can be expressed with an undetermined coefficient $k_{1\sim4}$ as [12]:

$$\Delta i_d = k_1 \sin(\omega_e t) + k_2 \sin(2\omega_e t) + o_d, \tag{10}$$

$$\Delta i_q = k_3 \cos(\omega_e t) + k_4 \cos(2\omega_e t) + o_q, \tag{11}$$

From the above analysis, it can be seen that the main disturbance components in the PM servo system can be divided as follows: (1) the constant disturbances caused by the parameter mismatch of resistance, inductance, and moment of inertia; (2) disturbances with a frequency of $6\omega_e$ caused by the flux harmonics and dead-time effect; and (3) disturbances with a frequency of $\omega_e$ and $2\omega_e$ caused by current sampling errors.

### 3. Design of Nonlinear Predictive Speed Controller

*3.1. Continuous-Time Predictive Model*

The dynamic model of the PM servo system in the d-q frame can be expressed as [39]:

$$u_{\text{sd}} = R_s i_{\text{sd}} + L_d \frac{di_{\text{sd}}}{dt} - L_q n_p \omega_m i_{\text{sq}}, \tag{12}$$

$$u_{\text{sq}} = R_s i_{\text{sq}} + L_q \frac{di_{\text{sq}}}{dt} + L_d n_p \omega_m i_{\text{sd}} + n_p \omega_m \psi_f, \tag{13}$$

$$J_m \frac{d\omega_m}{dt} = T_e - T_L - B\omega_m, \tag{14}$$

Considering the disturbance factors in (12)–(14), then we can obtain:

$$\dot{x}(t) = f(t) + g_1 u(t) + g_2(\chi_c(t) + \chi_h(t)), \tag{15}$$

where $x = [i_{\text{sd}} \; i_{\text{sq}} \; \omega_m]^T$, $u = [u_{\text{sd}} \; u_{\text{sq}}]^T$,

$$\chi_c(t) = \begin{bmatrix} \Delta R i_{\text{sd}} + \Delta L_d(di_{\text{sd}}/dt) - n_p \omega_m \Delta L_q i_{\text{sq}} \\ \Delta R i_{\text{sq}} + \Delta L_q(di_{\text{sq}}/dt) + n_p \omega_m \Delta L_d i_{\text{sd}} \\ T_L + B\omega_m + \Delta J(d\omega_m/dt) \end{bmatrix},$$

$$\chi_h(t) = \begin{bmatrix} -\Delta u_d + \Delta i_{\text{sd}}(R_s + \Delta R) + (L_d + \Delta L_d)(d\Delta i_{\text{sd}}/dt) \\ -n_p \omega_m (L_q + \Delta L_q)\Delta i_{\text{sq}} \\ \overline{-\Delta u_q + \Delta i_{\text{sq}}(R_s + \Delta R) + (L_q + \Delta L_q)(d\Delta i_{\text{sq}}/dt)} \\ +n_p \omega_m (L_d + \Delta L_d)\Delta i_{\text{sd}} + p_r \omega_m \psi_{fd} \\ 1.5 p_r \begin{bmatrix} -i_{\text{sq}} \sum_{l=1}^{\infty} \psi_{d6,l} \cos(6l\omega_e t) + \psi_{d0}\Delta i_q - \\ (L_d - L_q)i_{\text{sd}}\Delta i_q - (L_d - L_q)i_{\text{sq}}\Delta i_d \end{bmatrix} \end{bmatrix}.$$

The other coefficient matrices are:

$$f(t) = \begin{bmatrix} f_d \\ f_q \\ f_w \end{bmatrix} = \begin{bmatrix} (-R_s i_{\text{sd}} + n_p \omega_m L_q i_{\text{sq}})/L_d \\ (-R_s i_{\text{sq}} - n_p \omega_m L_d i_{\text{sd}} - p_r \omega_m \psi_f)/L_q \\ \{1.5 n_p [\psi_{d0} i_{\text{sq}} + (L_d - L_q)i_{\text{sd}} i_{\text{sq}}] - B\omega_m\}/J_m \end{bmatrix}, \; g_1 = \begin{bmatrix} 1/L_d & 0 \\ 0 & 1/L_q \\ 0 & 0 \end{bmatrix},$$

$$g_2 = \begin{bmatrix} -1/L_d & 0 & 0 \\ 0 & -1/L_q & 0 \\ 0 & 0 & -1/J_m \end{bmatrix}.$$

It can be seen from (20) that $\chi_c(t)$ is mainly introduced by parameter mismatch and external load disturbance, and $\chi_h(t)$ is mainly introduced by the dead-time effects and current sampling errors. Taking the disturbance frequency as the modeling characteristic, the nonlinear model of PM servo system can be constructed as:

$$\begin{cases} \dot{x}(t) = f(t) + g_1 u(t) + g_2 \chi(t) \\ y(t) = h(x) \end{cases}, \tag{16}$$

where $\chi(t) = \chi_c(t) + \chi_h(t)$, $h(x) = [h_1 \; h_2 \; h_3]^T = [i_{\text{sd}} \; i_{\text{sq}} \; \omega_m]^T$

*3.2. Long-Horizon Optimization and Its Control Law*

From (17)–(19), the relative order of $i_{\text{sd}}$ and $i_{\text{sq}}$ is equal to 1, and the relative order of $\omega_m$ is equal to 2. Then, we can obtain:

$$i_{\text{sd}}(t + \tau) = i_{\text{sd}}(t) + \tau \dot{i}_{\text{sd}}(t), \tag{17}$$

$$i_{\text{sq}}(t + \tau) = i_{\text{sq}}(t) + \tau \dot{i}_{\text{sq}}(t), \tag{18}$$

$$\omega_m(t + \tau) = \omega_m(t) + \tau \dot{\omega}_m(t) + \frac{\tau^2}{2} \ddot{\omega}_m(t), \tag{19}$$

where:

$$\begin{cases} \dot{i}_{\text{sd}}(t) = L_f i_{\text{sd}} + L_{g_1} i_{\text{sd}} u(t) + L_{g_2} i_{\text{sd}} \chi(t) \\ \dot{i}_{\text{sd/q}}(t) = L_f i_{\text{sq}} + L_{g_1} i_{\text{sq}} u(t) + L_{g_2} i_{\text{sq}} \chi(t) \end{cases}, \tag{20}$$

$$\dot{\omega}_{\text{m}}(t) = L_f \omega_{\text{m}} + L_{g_2} \omega_{\text{m}} \chi(t), \tag{21}$$

$$\ddot{\omega}_{\text{m}}(t) = L_f^2 \omega_{\text{m}} + L_{g_1} L_f \omega_{\text{m}} u(t) + L_{g_2} L_f \omega_{\text{m}} \chi(t), \tag{22}$$

To evaluate the tracking performance of output variables in the future time scale, the cost function is defined as:

$$J = \frac{1}{2} \int_0^{T_i} q_i \left\{ \begin{array}{c} \left[ i_{\text{sd}}^{\text{ref}}(t+\tau) - i_{\text{sd}}(t+\tau) \right]^2 \\ + \left[ i_{\text{sq}}^{\text{ref}}(t+\tau) - i_{\text{sq}}(t+\tau) \right]^2 \end{array} \right\} \mathrm{d}\tau + \frac{1}{2} \int_0^{T_w} q_w \left[ \omega_{\text{m}}^{\text{ref}}(t+\tau) - \omega_{\text{m}}(t+\tau) \right]^2 \mathrm{d}\tau, \tag{23}$$

Substituting (20)–(22) into (23), then we obtain:

$$J = \frac{1}{2} \left[ \overline{\boldsymbol{Y}}(t) - \overline{\boldsymbol{W}}(t) \right]^{\text{T}} \overline{\boldsymbol{H}}(\tau) \left[ \overline{\boldsymbol{Y}}(t) - \overline{\boldsymbol{W}}(t) \right], \tag{24}$$

where:

$$\overline{\boldsymbol{Y}}(t) = \begin{bmatrix} i_{\text{sd}} & \dot{i}_{\text{sd}} & i_{\text{sq}} & \dot{i}_{\text{sq}} & \omega_{\text{m}} & \dot{\omega}_{\text{m}} & \ddot{\omega}_{\text{m}} \end{bmatrix}^{\text{T}},$$
$$\overline{\boldsymbol{W}}(t) = \begin{bmatrix} i_{\text{sd}}^{\text{ref}} & \dot{i}_{\text{sd}}^{\text{ref}} & i_{\text{sq}}^{\text{ref}} & \dot{i}_{\text{sq}}^{\text{ref}} & \omega_{\text{m}}^{\text{ref}} & \dot{\omega}_{\text{m}}^{\text{ref}} & \ddot{\omega}_{\text{m}}^{\text{ref}} \end{bmatrix}^{\text{T}},$$
$$\overline{\boldsymbol{H}}(\tau) = \text{diag}\begin{pmatrix} q_i \int_0^{T_i} H_1^{\text{T}} H_1 \mathrm{d}\tau, q_i \int_0^{T_i} H_2^{\text{T}} H_2 \mathrm{d}\tau, \\ q_w \int_0^{T_i} H_3^{\text{T}} H_3 \mathrm{d}\tau \end{pmatrix}, H_1 = H_2 = \begin{bmatrix} 1 & \tau \end{bmatrix}, H_3 = \begin{bmatrix} 1 & \tau & \tau^2/2 \end{bmatrix}.$$

According to the unconstrained quadratic optimization theory [36], the optimal solution of the optimization problem corresponding to cost function (24) is equivalent to $\partial J / \partial \boldsymbol{u} = 0$; then, we can obtain the corresponding law of the nonlinear predictive speed controller (NPSC), i.e.,

$$\boldsymbol{u}(t) = -\boldsymbol{G}^{-1} \boldsymbol{M} [\boldsymbol{Y} - \boldsymbol{W} + \boldsymbol{N} \chi(t)], \tag{25}$$

where:

$$\boldsymbol{G} = \frac{q_i T_i^3}{3} \left[ L_{g_1}^{\text{T}} i_{\text{d}} L_{g_1} i_{\text{d}} + L_{g_1}^{\text{T}} i_{\text{q}} L_{g_1} i_{\text{q}} \right] + \frac{q_w T_w^3}{20} L_{g_1} L_f^{\text{T}} \omega_{\text{m}} L_{g_1} L_f \omega_{\text{m}},$$

$$\boldsymbol{M} = \begin{bmatrix} q_i T_i^2 L_{g_1}^{\text{T}} i_{\text{d}}/2 & q_i T_i^3 L_{g_1}^{\text{T}} i_{\text{d}}/3 & q_i T_i^2 L_{g_1}^{\text{T}} i_{\text{q}}/2 & q_i T_i^3 L_{g_1}^{\text{T}} i_{\text{q}}/3 \\ q_w T_i^3 L_{g_1} L_f^{\text{T}} \omega_{\text{m}}/6 & q_w T_i^4 L_{g_1} L_f^{\text{T}} \omega_{\text{m}}/8 & q_w T_i^5 L_{g_1} L_f^{\text{T}} \omega_{\text{m}}/20 \end{bmatrix}$$

$$\boldsymbol{Y} = \begin{bmatrix} L_f^0 i_{\text{sd}} & L_f^1 i_{\text{sd}} & L_f^0 i_{\text{sq}} & L_f^1 i_{\text{sd}} & L_f^0 \omega_{\text{m}} & L_f^1 \omega_{\text{m}} & L_f^2 \omega_{\text{m}} \end{bmatrix}^{\text{T}},$$

$$\boldsymbol{W} = \begin{bmatrix} i_{\text{sd}}^{\text{ref}} & \dot{i}_{\text{sd}}^{\text{ref}} & i_{\text{sq}}^{\text{ref}} & \dot{i}_{\text{sq}}^{\text{ref}} & \omega_{\text{m}}^{\text{ref}} & \dot{\omega}_{\text{m}}^{\text{ref}} & \ddot{\omega}_{\text{m}}^{\text{ref}} \end{bmatrix}^{\text{T}},$$

$$\boldsymbol{N} = \begin{bmatrix} \boldsymbol{O} & L_{g2} i_{\text{sd}} & \boldsymbol{O} & L_{g2} i_{\text{sq}} & \boldsymbol{O} & L_{g2} \omega_{\text{m}} & L_{g2} L_f \omega_{\text{m}} \end{bmatrix}^{\text{T}}.$$

where $\boldsymbol{O}$ is the zero matrix.

### 3.3. Asymptotic Stability Analysis

Assuming that $\chi(t)$ and its derivatives are continuous and bounded, $\chi(t)$ can be estimated by constructing a disturbance observer. Therefore, on the premise of ignoring the influence of disturbance, by substituting (25) into (15), we can obtain:

$$\dot{\boldsymbol{e}} = \begin{bmatrix} -\frac{3}{2T_i} & 0 & 0 & 0 \\ 0 & -\frac{3}{2T_i} & -\frac{q_w n_p \psi_f}{2J_m} & -\frac{3q_w n_p \psi_f}{8J_m} \\ 0 & 0 & 0 & 1 \\ 0 & -\frac{10 q_i J_m}{n_p \psi_f T_i^3} & -\frac{10}{3T_w^2} & -\frac{5}{2T_w} \end{bmatrix} \boldsymbol{e}, \tag{26}$$

where $e = \begin{bmatrix} i_{sd} - i_{sd}^{ref} & i_{sq} - i_{sq}^{ref} & \omega_m - \omega_m^{ref} & \dot{\omega}_m - \dot{\omega}_m^{ref} \end{bmatrix}^T$.

From (26), the characteristic polynomial of system is:

$$\begin{cases} \left(s + \frac{3}{2T_i}\right)^2 = 0 \\ s^2 + \frac{5}{2T_w}s + \frac{10}{3T_w^2} = 0 \end{cases}, \tag{27}$$

From (27), the solutions of the characteristic polynomial are $s_{1,2} = -3/2T_i$, $s_{3,4} = (-1.25 \pm j1.307)/T_w$. Because the predictive horizon $T_i$ and $T_w$ are positive, the eigenvalues are located in the left plane of the complex plane, which means the designed system is stable.

It can also be seen from Equation (27) that NPSC has four system characteristic roots, which correspond to the current and speed control performance of the d-axis and q-axis, respectively. Among these, the current control performance is approximately equal to the first-order controller, and the speed control performance is approximately equal to the under-damped second-order controller. In addition, the dynamic regulation time of speed is usually longer than the control period; as a result, it is necessary to implement multi-step prediction for predictive speed control to ensure the stability of the algorithm, and the predictive horizon is required to cover the dynamic process of speed. Thus, $T_w > T_i$, which shows that the current dynamic performance of NPSC is better than that of speed. Furthermore, with the increase in $T_i$ and $T_w$, the eigenvalues of the system are closer to the imaginary axis of the complex plane, and the dynamic process of the system slows accordingly. To summarize, the values of $T_i$ and $T_w$ should not be selected as being too large or too small to ensure the stability of system.

The high bandwidth is the key element for high-performance control of NPSC. Hence, it is necessary to undertake quantitative analysis of the actual bandwidth of NPSC. Employing the transformation results of $i_d^{ref}$, $i_d$, $\omega_e^{ref}$, and $\omega_e$ in the Laplace domain, $I_d^{ref}(s)$, $I_d(s)$, $W^{ref}(s)$, and $W(s)$, the control bandwidth of the proposed strategy is analyzed as follows:

$$\begin{cases} \frac{I_d^{ref}(s)}{I_d(s)} = 1 + \frac{1}{6}T_i s \\ \frac{W^{ref}(s)}{W(s)} = \frac{K^*\left[2q_w T_i T_w^5 s^2 + \left(12q_w T_w^5 + 5q_w T_i T_w^4\right)s + 30q_w T_w^4\right]}{2q_w T_i T_w^5 s^2 + \left(12q_w T_w^5 + 5q_w T_i T_w^4\right)s + 30q_w T_w^4 + 240J} \end{cases}, \tag{28}$$

It can be seen from (28) that NPSC is essentially a type of PD controller for the d-axis current control. The control characteristics are externally manifested as an all-pass characteristic, which has high-control bandwidth and poor noise suppression. However, the application of the following harmonic disturbance observer (HDO) can effectively compensate for this defect. For the speed control part, HDO-NPSC is approximately equivalent to a class of P-type controller. Similarly, HDO is used to suppress harmonics in the control system.

## 4. Harmonic Disturbance Observer

### 4.1. Modified Observer Targeting at Harmonics Estimation

There are still unknown disturbances in the optimal control law shown in (25), with the exceptions of the given nominal parameters, predetermined control parameters, and predictive horizon. According to the construction principle of the nonlinear observer [40], the disturbance observer with (16) can be constructed as:

$$\begin{cases} \dot{\hat{\chi}}(t) = L\left(\chi(t) - \hat{\chi}(t)\right) \\ \chi(t) = g_2^{-1}\left(-f(t) - g_1 u(t)\right) \end{cases}, \tag{29}$$

From (34), the nonlinear observer converges when $\dot{\hat{\chi}}(t) = 0$, which means $\hat{\chi}(t) \to \chi(t)$. That is, the classical nonlinear observer can only observe the constant or slowly varying

disturbances. However, not only are constant disturbances $\chi_c(t)$ present in the PM servo system, but also harmonic disturbances $\chi_h(t)$.

To observe the harmonic disturbances with frequencies of $\omega_e$, $2\omega_e$, and $6\omega_e$, which are denoted as $\chi_h(t)$, $\chi_{2h}(t)$, and $\chi_{6h}(t)$, $\chi(t)$ can be reconstructed according to the different disturbance frequencies, as:

$$\dot{\xi} = X\zeta = \begin{bmatrix} O & & & \\ & X(\omega_e) & & \\ & & X(2\omega_e) & \\ & & & X(6\omega_e) \end{bmatrix} \xi, \tag{30}$$

where: $X(\omega_e) = \begin{bmatrix} & & & I_3 \\ -\omega_e^2 & & & \\ & -\omega_e^2 & & \\ & & -\omega_e^2 & \end{bmatrix}$ ,

$\xi = \begin{bmatrix} \chi_c & \chi_h(t) & \dot{\chi}_h(t) & \chi_{2h}(t) & \dot{\chi}_{2h}(t) & \chi_{6h}(t) & \dot{\chi}_{6h}(t) \end{bmatrix}^T$.

Combined with (16) and (30), the modified nonlinear disturbance observer can be contrasted as:

$$\begin{cases} \dot{\hat{\xi}} = X\hat{\zeta} + Lg_2\left(\chi(t) - \hat{\chi}(t)\right) \\ \chi(t) = g_2^{-1}(\dot{x} - f(t) - g_1u(t)) \\ \hat{\chi}(t) = C\hat{\zeta} \end{cases}, \tag{31}$$

where $C = [\mathbf{1}_{1\times 3}\ \mathbf{1}_{1\times 3}\ 0\ \mathbf{1}_{1\times 3}\ 0\ 1\ 0]$, $\mathbf{1}_{1\times 3}$ is the ones matrix, and $L = [\ L_c\ L_h\ L_{2h}\ L_{6h}]^T$ is the coefficient matrix of the observer.

### 4.2. Stability of Modified Observer

The observation errors are defined as $\varepsilon = \xi - \hat{\xi}$; then, the following equation can be obtained according to (31):

$$\dot{\varepsilon} = (X - Lg_2C)\varepsilon, \tag{32}$$

and the Lyapunov function is defined as follows:

$$V = \varepsilon^T P\varepsilon, \tag{33}$$

where $P$ is an arbitrary symmetric positive definite matrix. The derivative of the Lyapunov function is:

$$\dot{V} = \varepsilon^T P\dot{\varepsilon} + \dot{\varepsilon}^T P\varepsilon = \varepsilon^T \left[ P(X - Lg_2C) + (X - Lg_2C)^T P \right] \varepsilon, \tag{34}$$

For the nonlinear disturbance observer in (37), it can be seen from (36) and (37) that there is always an observer coefficient matrix $L$ which makes $P(X - Lg_2C)$ negative definite. That is, the observation errors $\varepsilon \to 0$, $\hat{\xi} \to \xi$ when $t \to \infty$.

Since the derivative information of the state variables is difficult to obtain, we can solve this problem by introducing the relationship of $\hat{\xi} = z + p(x)$ into (37). Finally, the mathematical expression of HDO is constructed as:

$$\begin{cases} \dot{z} = (X - Lg_2C)z + Xp(x) - Lf(t) - \\ \qquad Lg_1u(t) - Lg_2Cp(x) \\ \hat{\chi}(t) = C[z + p(x)] \\ p(x) = Lx \end{cases}, \tag{35}$$

## 5. Proposed Scheme and Its Parameter Tuning

From substituting the estimated value in (35) into (25), the principal block diagram of HDO-NPSC can be shown as in Figure 1.
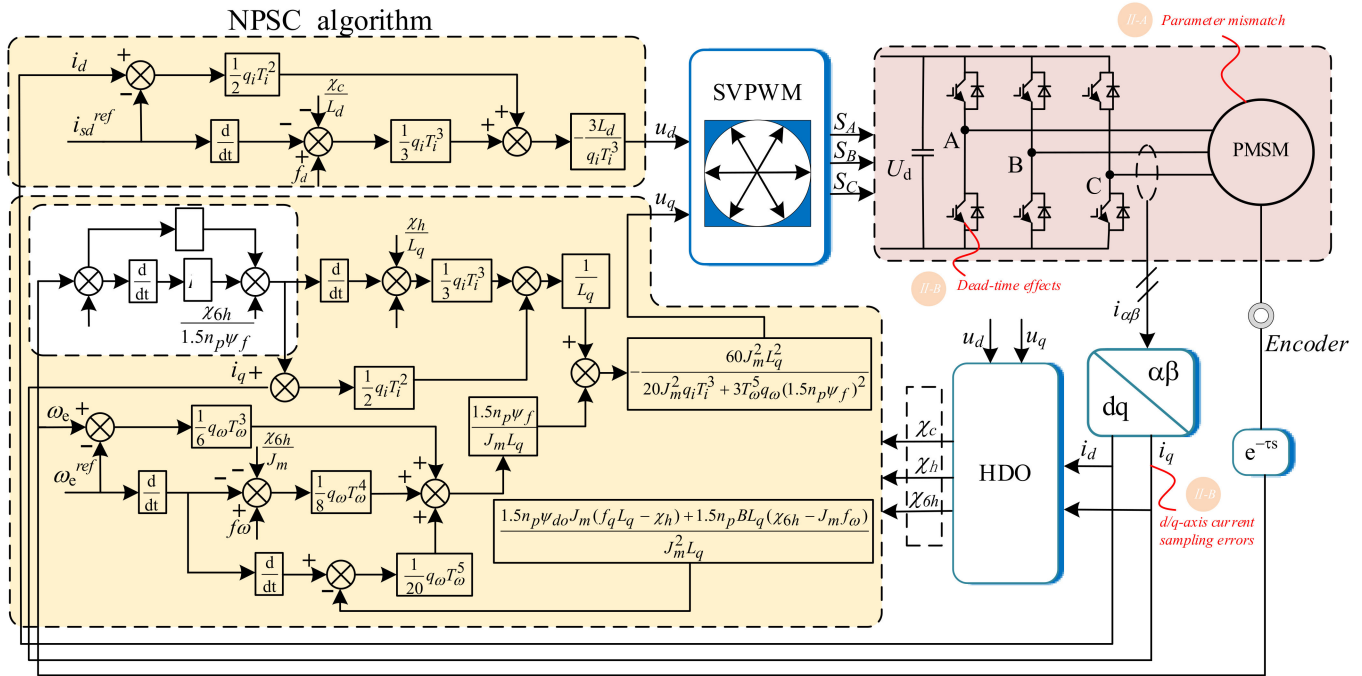


**Figure 1.** Control block diagram of the proposed HDO-NPSC.

In the proposed algorithm, $i_{\text{sd}}{}^{\text{ref}} = 0$. Furthermore, an additional PD controller is introduced to adjust the relationship between the q-axis reference current and the speed; its expression is:

$$i_{\text{sq}}^{\text{ref}} = \begin{bmatrix} 0 & 0 & 1/1.5n_p\psi_f \end{bmatrix} \hat{\chi}(t) + K_{\text{p}}\left(\omega_{\text{m}}^{\text{ref}} - \omega_{\text{m}}\right) + K_{\text{d}}\left(\dot{\omega}_{\text{m}}^{\text{ref}} - \dot{\omega}_{\text{m}}\right), \tag{36}$$

where $K_{\text{p}}$ and $K_{\text{d}}$ are the proportional and differential coefficients, respectively. The PD controller is employed to modify the reference value of the q-axis current in advance to ensure the dynamic performance, but it does not change the control structure and stability of HDO-NPSC.

From the system model in (15), state errors in (26), and observation errors in (32), it can be concluded that:

$$\begin{bmatrix} \dot{e} \\ \dot{\varepsilon} \end{bmatrix} = \left[\begin{array}{cccc:c} -\dfrac{3}{2T_{\text{i}}} & 0 & 0 & 0 & \\ 0 & -\dfrac{3}{2T_{\text{i}}} & -\dfrac{q_{\text{w}}n_{\text{p}}\psi_{\text{f}}}{2J_{\text{m}}} & -\dfrac{3q_{\text{w}}n_{\text{p}}\psi_{\text{f}}}{8J_{\text{m}}} & \boldsymbol{B} \\ 0 & 0 & 0 & 1 & \\ 0 & -\dfrac{10q_i J_{\text{m}}}{n_{\text{p}}\psi_{\text{f}}T_{\text{i}}^3} & -\dfrac{10}{3T_{\text{w}}^2} & -\dfrac{5}{2T_{\text{w}}} & \\ \hdashline & & & & \boldsymbol{X} - \boldsymbol{L}_{\varepsilon}\boldsymbol{g}_2\boldsymbol{C} \end{array}\right] \begin{bmatrix} e \\ \varepsilon \end{bmatrix}, \tag{37}$$

In (37), $\boldsymbol{B}$ is a parameter matrix independent of $\boldsymbol{L}$. The control parameters of NPSC are the current weight $q_{\text{i}}$ and predictive horizon $T_{\text{i}}$, and speed weight $q_{\text{w}}$ and predictive horizon $T_{\text{w}}$. The control parameters of HDO are contained in the coefficient matrix $\boldsymbol{L}$. From (37), it can be found that HDO and NPSC can be designed separately, and there is no direct parameter coupling relationship between them. Therefore, the parameter design of

NPSC can be completed under the assumption that $\chi(t) = 0$, and then $L$ can be adjusted based on the pole assignment of the NPSC-based system. The specific parameter tuning process is shown in Figure 2.
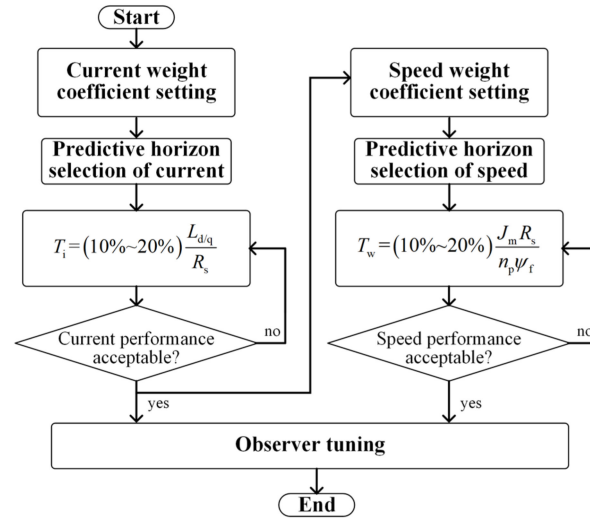


**Figure 2.** Parameter tuning flowchart of the proposed HDO-NPSC.

According to the flowchart of Figure 2, the detailed parameter setting procedure is listed as follows:

Step I: Current control parameters. The parameters of the current control part should be set first in the case of disconnecting the speed control part (i.e., set $i_{sq}{}^{ref}$ to a fixed value and block the output of the PD controller). The specific parameter tuning process is as follows. Firstly, the current horizon $T_i$ within the allowable range should be selected to set the current weight coefficient (e.g., $T_i = T_s$ is also allowed). The setting process of the current weight coefficient is completed until the motor system can operate normally and the q-axis current can track the given value. Then, the current horizon should be optimized under the condition of keeping the current weight coefficient unchanged. It is worth mentioning that the speed predictive horizon should be selected to be sufficiently long to cover the dynamic process of the motor system as much as possible. However, it can be seen from Section 3.3 that a predictive horizon having a too-large value will lead to dynamic performance degradation. For this reason, the current predictive horizon is generally selected as 10%–20% of the transient time constant of servo system; then:

$$T_{id} = (10\% \sim 20\%)\frac{L_d}{R_s}, T_{iq} = (10\% \sim 20\%)\frac{L_q}{R_s}, \tag{38}$$

Step II: Speed Control Parameters. Similarly, the speed predictive horizon is generally selected as:

$$T_w = (10\% \sim 20\%)\frac{J_m R_s}{n_p \psi_f}, \tag{39}$$

The weight coefficient determines the importance of each variable in the control process; however, a too-large value will destroy the stability of the system. Therefore, it is necessary to gradually increase the value of $q_w$ from a smaller value until a satisfactory control effect is achieved.

Step III: Observer parameters. To ensure the observation speed and interference suppression performance, the observer poles are usually assigned to be 2~5 times faster than the system poles.

## 6. Experimental Results

To verify the feasibility and effectiveness of NDO-NPSC, the experiments were carried out on a 2.3 kW surface-mounted PMSM. The parameters of the motor are given in Table 1. In the testbench, the load torque is produced by a PM servo motor of the same model. In the following experiments, the algorithms were implemented with a TMS320F28377D micro controller unit (MCU) produced by TI and a Cyclone V FPGA produced by Intel. DSP was used to execute the code of the main algorithm, and FPGA was used to implement the high-precision analog-to-digital conversion (ADC), digital-to-analog conversion (DAC), and pulse generation.

**Table 1.** PMSM parameters.

| Parameter | Symbol | Value |
|---|---|---|
| Rated power | $P_N$ | 2.3 kW |
| Number of pole-pairs | $p$ | 2 |
| Rated speed | $n_N$ | 1500 r/min |
| Rated torque | $T_N$ | 15 Nm |
| Rated current | $I_N$ | 10 A |
| Permanent magnet flux | $\psi_r$ | 0.33 Wb |
| Stator resistance | $R_s$ | 0.63 $\Omega$ |
| Stator inductance | $L_s$ | 4.0 mH |
| Moment of inertia | $J_m$ | 0.00272 kg·m$^2$ |
| Control period | $T_s$ | 100 µs |

Figure 3 shows the steady-state experimental waveforms of the motor speed, current, and rotor position with the proposed HDO-NPSC. In the experiments, the operating performance of PMSM adopting HDO-NPSC under the condition of high/low speed with heavy/light load were verified. It can be seen from Figure 3 that the servo motor system can work stably at the given speed with load when HDO-NPSC is adopted. The proposed HDO-NPSC algorithm can achieve favorable speed tracking performance regardless of high/low speed and light/heavy load conditions. At the low speed and light load condition, the low-frequency harmonics introduced by non-ideal flux harmonics are more significant and the three-phase current has slight distortion. However, the overall steady-state control performance is still excellent.
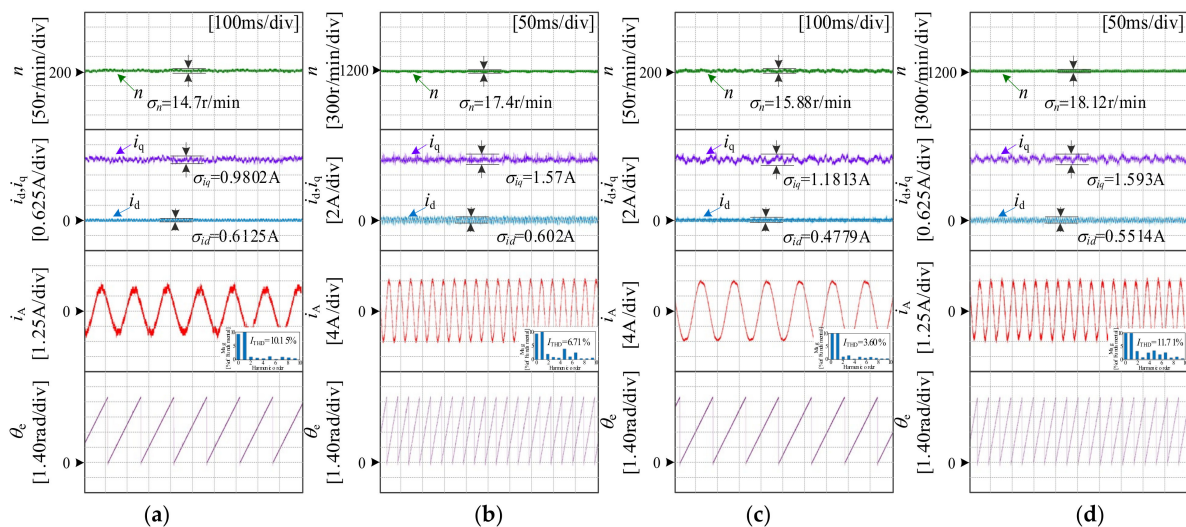


**Figure 3.** Experimental results of the proposed algorithm under the steady-state operation. (**a**) Low speed (200 r/min) with light-load condition (3.75 Nm). (**b**) High speed (1200 r/min) with heavy-load condition (12 Nm). (**c**) Low speed (200 r/min) with heavy-load condition (12 Nm). (**d**) High speed (1200 r/min) with light-load condition (3.75 Nm).

Figure 4 shows the dynamic experimental waveforms of speed, stator current, and rotor position of FOC with the Luenberger observer (DOB-FOC), predictive speed control with the Luenberger observer [41], and HDO-NPSC, respectively. In Figure 4, the rotor speed is accelerated abruptly from 0 to 800 r/min with no load; the given speed is then unchanged and the load torque is abruptly increased to 8.2 Nm. As shown in Figure 4, when the speed reference is a step signal, all three strategies can track the speed reference value without bias. The speed response time of DOB-FOC is 697.1 ms, whereas that of DOB-PSC is 43.5 ms and that of HDO-NPSC is 204 ms. More importantly, when load disturbance occurs, the speed recovery time of DOB-FOC is 65 ms and that of DOB-PSC is 319.2 ms, whereas that of HDO-NPSC is 40.2 ms. Furthermore, comparing the $q$-axis current waveforms of the three methods, it can be seen that the $q$-axis current waveform of HDO-NPSC is relatively stable.
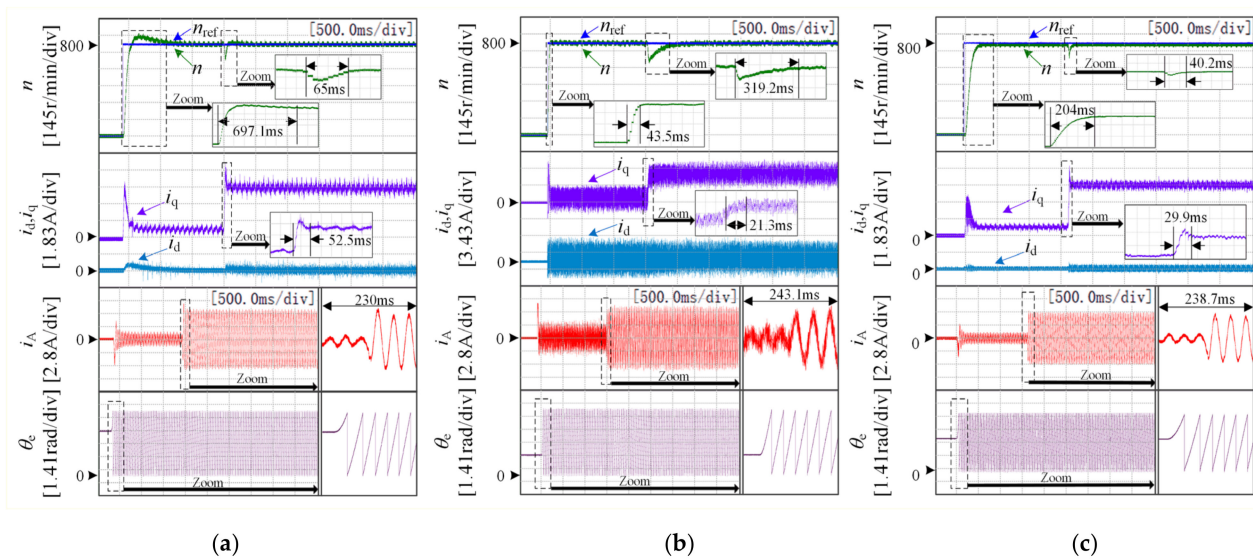


**Figure 4.** Comparison results of the proposed algorithm with DOB-FOC and DOB-PSC. (**a**) DOB-FOC. (**b**) DOB-PSC. (**c**) HDO-NPSC.

Furthermore, in order to comprehensively verify the performance of the proposed algorithm, the above three strategies without auxiliary observers were been compared. By comparing Figures 4 and 5, it can be found that, after adding the observer, the dynamic performance of FOC is indeed improved, but it is still inferior to HDO-NPSC. When the observer is removed, the prediction algorithms (PSC and NPSC) have some small steady-state errors. However, the dynamic performance of the proposed algorithm is satisfactory in the absence of an observer. In general, compared with the existing strategies, the proposed algorithm can significantly improve the dynamic performance of the motor system without increasing the cost of the control hardware and deteriorating the steady-state performance of the motor system.

Figure 6 shows the dynamic experimental waveforms of speed, stator current, and rotor position of HDO-NPSC, FOC (with the feedforward and anti-windup link), and PI-PCC, respectively. In Figure 6, the given speed of the servo motor system is set to a triangular wave with a peak value of 800 r/min with no external load. After a period of time, the load torque is abruptly increased to 8.2 Nm. From Figure 6, it can be seen that the proposed HDO-NPSC algorithm has better dynamic performance and faster response to the slope reference signal compared with the FOC and PI-PCC strategies. More importantly, it can also effectively avoid the tracking errors caused by the saturation effect of the PI controller. However, HDO-NPSC has a slight tracking error due to the lack of an integral link. This error is relatively small, and within the acceptable range for applications. From Figure 6, for the given signal of triangular wave speed, it can be seen more intuitively that

HDO-NPSC has smaller tracking error and faster response speed when tracking the given signal of a high type, which has obvious advantages.
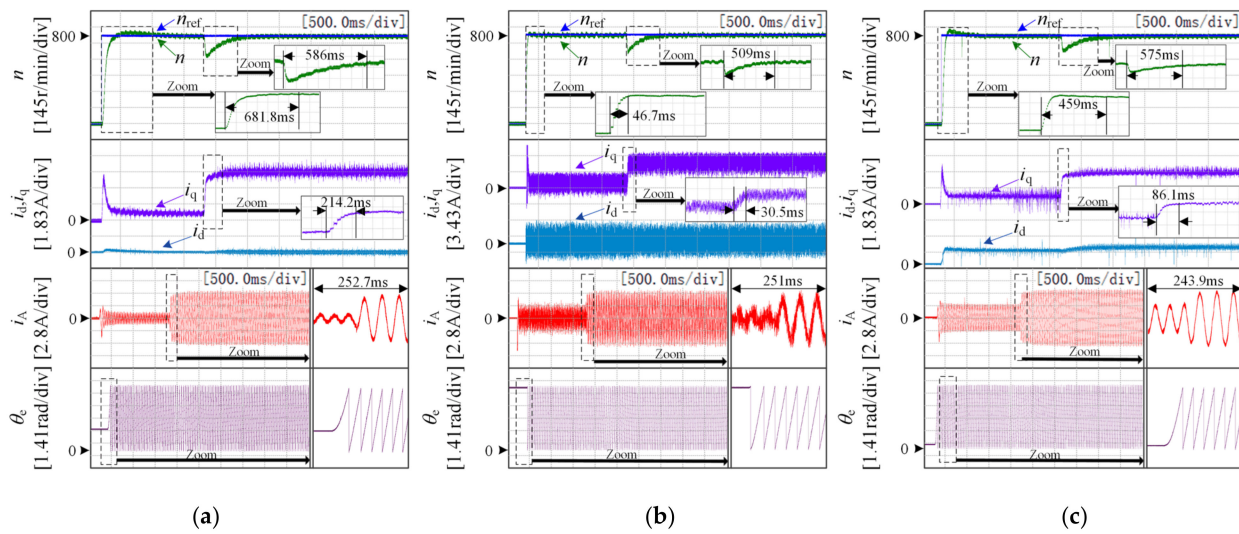


**Figure 5.** Comparison results of the proposed algorithm with FOC and PSC; all strategies are not equipped with observers. (**a**) FOC. (**b**) PSC. (**c**) NPSC.
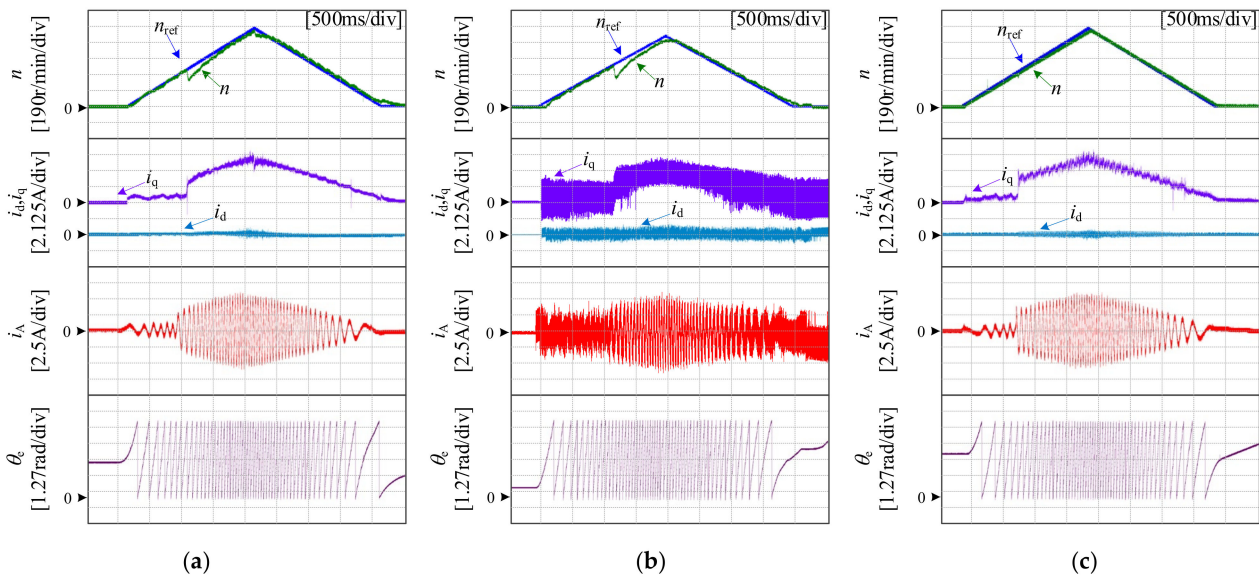


**Figure 6.** Tracking performance validation with triangular reference signals. (**a**) FOC (with the feedforward and anti-windup link). (**b**) PI-PCC. (**c**) HDO-NPSC.

## 7. Conclusions

An HDO-NPSC strategy for the PM servo system is presented in this paper. By separating the disturbance terms from the mathematical model of the system, a high-bandwidth nonlinear speed controller with non-cascaded structure was constructed, and the matching harmonic disturbance observer was designed to improve the anti-interference ability of the controller. Furthermore, the PD controller was employed to eliminate the traditional limitation loop, which further improves the tracking ability of the predictive speed algorithm for the high-type reference signals, e.g., the ramping signals and acceleration signal. To summarize, HDO-NPSC effectively solves the problems of classical DPSC in terms of disturbance suppression and efficient operation. Specifically, compared with FOC, the dynamic performance of HDO-NPSC is significantly improved; and, compared with

PI-PCC, it can achieve more stable steady-state performance, which means it has great value for the promotion and application of the predictive algorithm in servo systems.

The algorithm in this paper has the following disadvantages, and thus needs to be further improved. The essence of the proposed algorithm is to observe the spectrum of the disturbance distribution in the system by applying HDO. On this basis, it can inject the corresponding compensation into the control quantity (d-axis and q-axis voltages), so as to improve the control performance of motor speed. In conclusion, the compensation values that are opposite to the system disturbance in phase will be injected into the d-axis and q-axis currents, which will lead to a certain amount of compensation harmonics in the three-phase current.

**Author Contributions:** Conceptualization, Z.Z. and S.Y.; methodology, Z.Z.; software, C.M.; validation, Z.Z., S.Y. and C.M.; formal analysis, Z.Z.; investigation, Z.Z.; resources, Z.Z.; data curation, G.Z.; writing—original draft preparation, Z.Z.; visualization, G.Z.; supervision, Q.G.; project administration, Q.G.; funding acquisition, Z.Z. and Q.G. All authors have read and agreed to the published version of the manuscript.

**Institutional Review Board Statement:** Not applicable.

**Informed Consent Statement:** Not applicable.

**Data Availability Statement:** Not applicable.

## Nomenclature

| | |
|---|---|
| $i, u, \psi_f, T_s$ | Current, voltage, flux linkage of rotor, control period |
| $\omega_e, \omega_m$ | Electric angular frequency, mechanical angular frequency |
| $R, L, J_m, J_{load}$ | Resistance, inductance, the moment of inertia, the moment of inertia of load |
| $p_r, B, T_L$ | Pole pairs, friction coefficient, load torque |
| $L_{ef}, H, B, S$ | Core length of stator winding, magnetic field intensity, magnetic flux density, calculation area |
| $M_{iron}, M_{shaft}, R_{iron}, r_{iron}, R_{shaft}$ | Core mass, the shaft mass, the inner radius of core, the outer radius of the core, the inner radius of shaft |
| $x, u, \chi, h$ | State vector, input vector, disturbance vector, output vector |
| $q, T$ | Weight coefficient, predictive horizon |
| $\tau, L$ | Future time scale, Lie derivative |
| $\xi, L$ | State variable of observer, coefficient matrix of observer |
| $K_p, K_d$ | Proportional and differential coefficien of PD controller |
| $\Delta, o$ | Incremental quantity of variables, high-order infinitesimal variable |
| A, B, C, d, q (subscript) | Variables under A-, B-, C-, d-, q-axis |
| dc, s, 0 (subscript) | DC bus variables, stator variables, nominal value |
| c, h (subscript) | Constant disturbances variables, harmonics variables |
| dead (subscript) | Variables related to dead-time effects |
| i, w (subscript) | Current control loop variables, speed control loop variables |
| ref, $\wedge$ (superscript) | Reference values, estimated values |

## References

1. Wu, G.; Huang, S.; Wu, Q.; Rong, F.; Zhang, C.; Liao, W. Robust Predictive Torque Control of N*3-Phase PMSM for High-Power Traction Application. *IEEE Trans. Power Electron.* **2020**, *35*, 10799–10809. [CrossRef]
2. Ping, Z.; Wang, T.; Huang, Y.; Wang, H.; Lu, J.G.; Li, Y. Internal Model Control of PMSM Position Servo System: Theory and Experimental Results. *IEEE Trans. Ind. Inform.* **2020**, *16*, 2202–2211. [CrossRef]
3. Tang, Z.; Akin, B. A New LMS Algorithm Based Deadtime Compensation Method for PMSM FOC Drives. *IEEE Trans. Ind. Appl.* **2018**, *54*, 6472–6484. [CrossRef]

4. ZWang, Z.; Chen, J.; Cheng, M.; Chau, K.T. Field-Oriented Control and Direct Torque Control for Paralleled VSIs Fed PMSM Drives with Variable Switching Frequencies. *IEEE Trans. Power Electron.* **2016**, *31*, 2417–2428.

5. Mendoza-Mondragón, F.; Hernández-Guzmán, V.M.; Rodríguez-Reséndiz, J. Robust Speed Control of Permanent Magnet Synchronous Motors Using Two-Degrees-of-Freedom Control. *IEEE Trans. Ind. Electron.* **2018**, *65*, 6099–6108. [CrossRef]

6. Garcia, C.; Rodriguez, J.; Silva, C.; Rojas, C.; Zanchetta, P.; Abu-Rub, H. Full Predictive Cascaded Speed and Current Control of an Induction Machine. *IEEE Trans. Energy Convers.* **2016**, *31*, 1059–1067. [CrossRef]

7. Cisneros, P.S.; Werner, H. A Velocity Algorithm for Nonlinear Model Predictive Control. *IEEE Trans. Control. Syst. Technol.* **2020**, *29*, 1310–1315. [CrossRef]

8. Karamanakos, P.; Geyer, T.; Kennel, R. Reformulation of the long-horizon direct model predictive control problem to reduce the computational effort. In Proceedings of the 2014 IEEE Energy Conversion Congress and Exposition (ECCE), Pittsburgh, PA, USA, 14–18 September 2014; pp. 3512–3519.

9. Hang, J.; Wu, H.; Zhang, J.; Ding, S.; Huang, Y.; Hua, W. Cost Function-Based Open-Phase Fault Diagnosis for PMSM Drive System with Model Predictive Current Control. *IEEE Trans. Power Electron.* **2021**, *36*, 2574–2583. [CrossRef]

10. Errouissi, R.; Ouhrouche, M.; Chen, W.H.; Trzynadlowski, A.M. Robust Cascaded Nonlinear Predictive Control of a Permanent Magnet Synchronous Motor with Antiwindup Compensator. *IEEE Trans. Ind. Electron.* **2012**, *59*, 3078–3088. [CrossRef]

11. Chen, W.H.; Ballance, D.J.; Gawthrop, P.J.; O'Reilly, J. A Nonlinear Disturbance Observer for Robotic Manipulators. *IEEE Trans. Ind. Electron.* **2000**, *47*, 932–938. [CrossRef]

12. Xia, C.; Liu, N.; Zhou, Z.; Yan, Y.; Shi, T. Steady-State Performance Improvement for LQR-Based PMSM Drives. *IEEE Trans. Power Electron.* **2018**, *33*, 10622–10632. [CrossRef]

13. Yang, J.; Chen, W.H.; Li, S.; Guo, L.; Yan, Y. Disturbance/Uncertainty Estimation and Attenuation Techniques in PMSM Drives—A. Survey. *IEEE Trans. Ind. Electron.* **2017**, *64*, 3273–3285. [CrossRef]

14. Wang, L.; Freeman, C.T.; Chai, S.; Rogers, E. Predictive-repetitive control with constraints: From design to implementation. *J. Process. Control* **2013**, *23*, 956–967. [CrossRef]

15. Gupta, M.; Lee, J.H. Period-robust repetitive model predictive control. *J. Process. Control* **2006**, *16*, 545–555. [CrossRef]

16. Zhou, Z.; Xia, C.; Yan, Y.; Wang, Z.; Shi, T. Disturbances Attenuation of Permanent Magnet Synchronous Motor Drives Using Cascaded Predictive-Integral-Resonant Controllers. *IEEE Trans. Power Electron.* **2018**, *33*, 1514–1527. [CrossRef]

17. Song, Z.; Zhou, F. Observer-Based Predictive Vector-Resonant Current Control of Permanent Magnet Synchronous Machines. *IEEE Trans. Power Electron.* **2019**, *34*, 5969–5980. [CrossRef]

18. Gao, Y.; Chong, K.T. The Explicit Constrained Min-Max Model Predictive Control of a Discrete-Time Linear System with Uncertain Disturbances. *IEEE Trans. Autom. Control* **2012**, *57*, 2373–2378. [CrossRef]

19. Köhler, J.; Soloperto, R.; Müller, M.A.; Allgöwer, F. A Computationally Efficient Robust Model Predictive Control Framework for Uncertain Nonlinear Systems. *IEEE Trans. Autom. Control* **2021**, *66*, 794–801. [CrossRef]

20. Türker, T.; Buyukkeles, U.; Bakan, A.F. A Robust Predictive Current Controller for PMSM Drives. *IEEE Trans. Ind. Electron.* **2016**, *63*, 3906–3914. [CrossRef]

21. Zhou, P.; Chai, T.Y.; Zhao, J.H. DOB Design for Nonminimum-Phase Delay Systems and Its Application in Multivariable MPC Control. *IEEE Trans. Circuits Syst. II Exp. Briefs* **2012**, *59*, 525–529. [CrossRef]

22. Liu, H.; Li, S. Speed Control for PMSM Servo System Using Predictive Functional Control and Extended State Observer. *IEEE Trans. Ind. Electron.* **2012**, *59*, 1171–1183. [CrossRef]

23. Chen, M.; Mei, R. Robust tracking control of uncertain nonlinear systems using disturbance observer. In Proceedings of the 2011 International Conference on System Science and Engineering, Macau, China, 8–10 June 2011; pp. 431–436.

24. Chen, W.-H. Harmonic Disturbance Observer for Nonlinear Systems. *J. Dyn. Syst. Meas. Control* **2003**, *125*, 114–117. [CrossRef]

25. Zhang, X.; He, Y. Robust Model Predictive Direct Speed Control for SPMSM Drives Based on Full Parameters and Load Observer. In Proceedings of the 2019 IEEE International Symposium on Predictive Control of Electrical Drives and Power Electronics (PRECEDE), Quanzhou, China, 31 May–2 June 2019; pp. 1–5.

26. Zhang, X.; He, Y. Direct Voltage-Selection Based Model Predictive Direct Speed Control for PMSM Drives without Weighting Factor. *IEEE Trans. Power Electron.* **2019**, *34*, 7838–7851. [CrossRef]

27. Yuan, X.; Zhang, S.; Zhang, C. Improved Model Predictive Current Control for SPMSM Drives with Parameter Mismatch. *IEEE Trans. Ind. Electron.* **2020**, *67*, 852–862. [CrossRef]

28. Wei, Y.; Wei, Y.; Sun, Y.; Qi, H.; Guo, X. Prediction Horizons Optimized Nonlinear Predictive Control for Permanent Magnet Synchronous Motor Position System. *IEEE Trans. Ind. Electron.* **2020**, *67*, 9153–9163. [CrossRef]

29. Tarczewski, T.; Grzesiak, L.M. Constrained State Feedback Speed Control of PMSM Based on Model Predictive Approach. *IEEE Trans. Ind. Electron.* **2016**, *63*, 3867–3875. [CrossRef]

30. Feng, W.; O'reilly, J.; Ballance, D.J. MIMO nonlinear PID predictive controller. *IEE Proc. Control Theory Appl.* **2002**, *149*, 203–208. [CrossRef]

31. Tavernini, D.; Vacca, F.; Metzler, M.; Savitski, D.; Ivanov, V.; Gruber, P.; Hartavi, A.E.; Dhaens, M.; Sorniotti, A. An Explicit Nonlinear Model Predictive ABS Controller for Electro-Hydraulic Braking Systems. *IEEE Trans. Ind. Electron.* **2020**, *67*, 3990–4001. [CrossRef]

32. Errouissi, R.; Ouhrouche, M.; Chen, W.H.; Trzynadlowski, A.M. Robust Nonlinear Predictive Controller for Permanent-Magnet Synchronous Motors with an Optimized Cost Function. *IEEE Trans. Ind. Electron.* **2012**, *59*, 2849–2858. [CrossRef]

33. Liu, X.D.; Li, K.; Zhang, Q.; Zhang, C. Single-loop Predictive Control of PMSM Based on Nonlinear Disturbance Observers. *Proc. CSEE* **2018**, *38*, 2153–2162.

34. ZSong, Z.; Zhang, Z.; Komurcugil, H.; Lee, C.H. Controller-Based Periodic Disturbance Mitigation Techniques for Three-Phase Two-Level Voltage-Source Converters. *IEEE Trans. Ind. Inform.* **2021**, *17*, 6553–6568.

35. Hao, Z.; Zhou, W.; Ji, T.; Huang, X.; Zhang, C. Multi-Objective Optimization of Double Primary Tubular Permanent Magnet Synchronous Linear Motor in Wide Temperature Range Environment Based on Pareto Front Method. *IEEE Access* **2020**, *8*, 207193–207203. [CrossRef]

36. Wang, S.J.; Lin, S. K Analytical prediction of the incremental inductance of the permanent magnet synchronous motors. *IEEE Trans. Magn.* **2004**, *40*, 2044–2046. [CrossRef]

37. Lian, C.; Xiao, F.; Gao, S.; Liu, J. Load Torque and Moment of Inertia Identification for Permanent Magnet Synchronous Motor Drives Based on Sliding Mode Observer. *IEEE Trans. Power Electron.* **2018**, *34*, 5675–5683. [CrossRef]

38. Hwang, S.H.; Kim, J.M. Dead Time Compensation Method for Voltage-Fed PWM Inverter. *IEEE Trans. Energy Convers.* **2010**, *25*, 1–10. [CrossRef]

39. Linder, A.; Kanchan, R.; Stolze, P.; Kennel, R. *Model-Based Predictive Control of Electric Drives*; Cuvillier Verlag: Gottingen, Germany, 2010.

40. Li, S.; Yang, J.; Chen, W.H.; Chen, X. *Disturbance Observer-Based Control: Methods and Applications*; CRC Press: Boca Raton, FL, USA, 2014.

41. Wang, H.; Zhang, S.; Liu, W.; Geng, Q.; Zhou, Z. Finite control-set model predictive direct speed control of a PMSM drive based on the Taylor series model. *IET Electr. Power Appl.* **2021**, *15*, 1452–1465. [CrossRef]